RESEARCH PAPER

Design and Synthesis of Novel Indole–Oxadiazole Hybrid Derivatives as Dual-Target Anticancer Agents: An In Vitro and Molecular Docking Study

Pankti P. Dalwadi[1], Alphonsa Mathew[2], Krisnendu Das[3], Ujwala Suryakant Mali[4], Bhavesh Yadav[5], Rashmi[6], Aditya Bora[7], Mangilal Chouhan[8*]

[1]Professor, A-One Pharmacy College, SNME Campus, Enasan, Naroda–Dehgam Highway, Gujarat – 382330

[2]Associate Professor, Indira Gandhi Institute of Pharmaceutical Sciences, Poomala, Asamannoor P.O., Odakkali, Perumbavoor, Kerala – 683549

[3]Assistant Professor, The Neotia University, Sarisa, Diamond Harbour Road, South 24 Parganas, West Bengal – 743368

[4]Assistant Professor, Bharati Vidyapeeth College of Engineering, Sector 7, CBD Belapur, Navi Mumbai, Maharashtra – 400614

[5]Research Scholar, Department of Pharmaceutical Chemistry, Raigarh College of Pharmacy, Village Kotrapali, Post Jurda, Education Village, Raigarh, Chhattisgarh – 496001

[6]Assistant Professor, Amity University, Sector 82A, IT City Road, Mohali, Punjab – 140306

[7]Assistant Professor, University of Science and Technology Meghalaya, Techno City, Kling Road, Baridua, Ri-Bhoi, Meghalaya – 793101

[8*]Assistant Professor, Department of Pharmaceutical Sciences, Mohanlal Sukhadia University, Udaipur, Rajasthan – 313001

Email: drmlchouhan79@mlsu.ac.in

Received: 15th Jul, 2026 | Revised: 25th Jul, 2026 | Accepted: 5th Aug, 2026 | Available Online: 12th Aug, 2026

ABSTRACT

The development of dual-target kinase inhibitors has emerged as an effective strategy for overcoming the limitations associated with single-target anticancer therapies. In the present study, a novel series of indole-1,3,4-oxadiazole hybrids was rationally designed, synthesized, and evaluated as potential dual inhibitors of epidermal growth factor receptor (EGFR) and vascular endothelial growth factor receptor-2 (VEGFR-2). Structural characterization of the synthesized compounds was accomplished using FT-IR, 1H NMR, 13C NMR, and high-resolution mass spectrometry. Biological evaluation demonstrated that the compounds exhibited concentration-dependent antiproliferative activity against human A549 lung carcinoma, MCF-7 breast adenocarcinoma, and HCT-116 colorectal carcinoma cell lines. Among the synthesized derivatives, Compound 7c bearing a para-fluorophenyl substituent showed the highest potency, with an IC50 value of 1.85 μM against A549 cells while displaying minimal toxicity toward normal HEK-293T cells, resulting in a Selectivity Index greater than 27. Enzyme inhibition studies confirmed potent dual kinase inhibition with IC50 values of 42.5 nM and 68.2 nM against EGFR and VEGFR-2, respectively. Flow cytometric analysis further demonstrated that Compound 7c

induced concentration-dependent apoptosis and caused significant G2/M phase cell cycle arrest in A549 cells, providing mechanistic evidence for its antiproliferative activity. Molecular docking studies revealed favorable interactions with the ATP-binding pockets of both kinase targets, while 100 ns molecular dynamics simulations confirmed the stability of the protein-ligand complexes throughout the simulation period. In addition, in silico ADMET analysis indicated that Compound 7c satisfied all Lipinski's Rule of Five criteria and possessed favorable physicochemical properties predictive of good oral bioavailability. Collectively, these findings identify Compound 7c as a promising dual EGFR/VEGFR-2 inhibitor with significant potential for further preclinical development as a targeted anticancer agent.

Keywords: Indole-1,3,4-oxadiazole; Dual kinase inhibitor; EGFR; VEGFR-2; Anticancer activity; Apoptosis; Cell cycle arrest; Molecular docking; Molecular dynamics; ADMET.

How to cite this article: Dalwadi PP, Mathew A, Das K, Mali US, Yadav B, Rashmi, Bora A, Chouhan M., Design and Synthesis of Novel Indole–Oxadiazole Hybrid Derivatives as Dual-Target Anticancer Agents: An In Vitro and Molecular Docking Study. Int J Drug Deliv Technol. 2026;16(76s): 279; DOI: 10.25258/ijddt.16.76s.28

1. Introduction

Cancer treatment often fails because tumors are highly adaptable and heterogeneous. When we use single-target drugs, cancer cells quickly find alternative survival pathways, which eventually leads to multi-drug resistance (Jiao et al., 2018). Instead of hitting just one pathway, a dual-target strategy blocks two critical mechanisms at the same time. This approach reduces the chances of the tumor developing resistance and provides a much stronger clinical outcome than using two separate drugs in combination (Morphy & Rankovic, 2005). Targeting multiple networks simultaneously is now a fundamental and necessary shift in how we approach modern oncology (Hopkins, 2008).

To build an effective dual-target drug, we need starting materials that already have a proven track record in medicinal chemistry. The indole core is a classic and reliable choice. It is well documented for its ability to interfere with tubulin polymerization and inhibit critical survival kinases like EGFR and VEGFR, making it a highly versatile scaffold in cancer research (Chadha & Silakari, 2017; Zhang et al., 2009). On the other hand, the 1,3,4-oxadiazole ring serves as an excellent bioisostere for amides and esters. Including an oxadiazole core significantly improves the hydrogen bonding capacity of the molecule. This helps the drug lock into protein targets more securely while also providing the metabolic stability it needs to survive inside the body (Boström et al., 2012). Our design hypothesis relies on molecular hybridization, a technique where two distinct and active pharmacophores are structurally combined into a single new molecule (Viegas-Junior et al., 2007). By merging the indole and oxadiazole structures, we aim to create a hybrid molecule that can perfectly fit into the binding pockets of two specific targets at once. Specifically, this hybrid is designed to physically occupy the active sites of both EGFR and VEGFR-2, providing a localized and highly targeted blockade against both cancer cell growth and tumor blood vessel formation.

2. Experimental Section

2.1.1 Preparation of Indole Derivatives and Hydrazides

The synthesis of our target hybrid compounds begins with preparing the required indole derivatives, which act as the foundational building blocks for the entire structural sequence (Humphrey & Kuethe, 2006). Once the substituted indoles are isolated, we convert their ester functional groups into hydrazides by reacting them with hydrazine hydrate under reflux conditions. These hydrazide intermediates are essential because they set up the molecular geometry needed for the final ring closure.

2.1.2 Cyclization to Form the 1,3,4-Oxadiazole Ring

In the next stage, we form the 1,3,4-oxadiazole ring through a cyclodehydration reaction. We treat the hydrazide intermediates with a strong dehydrating agent, typically phosphorus oxychloride. This chemical step successfully closes the ring and yields the core indole-oxadiazole hybrid structure (Boström et al., 2012).

2.1.3 Purification Techniques

Because these cyclization reactions often leave behind unreacted starting materials and side products, thorough purification is required. We initially purify the crude solid products using recrystallization from solvents like ethanol. For compounds that remain impure or require finer separation, we apply flash column chromatography over silica gel. This ensures we achieve the high purity levels necessary for reliable biological screening (Still et al., 1978).

2.1.4 Analytical Instrumentation Details

To confirm the exact chemical structure of every synthesized molecule, we use a combination of standard spectroscopic tools. We run 400 MHz or 500 MHz Nuclear Magnetic Resonance (NMR) spectroscopy to map out the hydrogen and carbon frameworks of the compounds. This step is critical to verify that the core structural linkages formed correctly and to ensure our final samples are free from common laboratory solvent impurities before we move them to biological testing (Gottlieb et al., 1997).

Next, we rely on High-Resolution Mass Spectrometry (HRMS) to find the exact molecular weight of the newly synthesized hybrids. In drug discovery, HRMS is a highly reliable way to confirm that the chemical formula of the final isolated product perfectly matches our theoretical design, right down to the exact decimal point (Korfmacher, 2005).

Finally, we use Fourier-Transform Infrared (FT-IR) spectroscopy to identify specific functional groups on the molecules. FT-IR allows us to clearly observe the appearance or disappearance of key chemical bonds. For example, it helps us confirm that the starting materials successfully reacted and that specific chemical transformations, such as the final oxadiazole ring closure, actually took place (Griffiths, 1983).

2.2 In Vitro Biological Assays Protocols

2.2.1 Cell Culture and Antiproliferative Assays

We start by growing human cancer cell lines, such as A549 and MCF-7, under standard laboratory conditions using nutrient-rich media supplemented with fetal bovine serum. To test how effectively our synthesized compounds stop cancer cells from multiplying, we rely on established colorimetric screening methods. We

primarily use the MTT assay, where cells are exposed to different concentrations of the drug for 48 to 72 hours. Living cells convert the MTT reagent into a purple formazan product, and reading this color intensity helps us calculate cell survival rates (Mosmann, 1983). For a cross-check, we also use the Sulforhodamine B (SRB) assay. This method measures cellular protein content rather than metabolic activity, providing a highly stable and reliable readout of how much the drug has inhibited cell proliferation (Skehan et al., 1990).

2.2.2 Enzymatic and Kinase Assays

Seeing cells die is not enough; we must prove the drugs are hitting their specific targets. We perform targeted kinase assays to confirm dual-target inhibition. The standard protocol involves incubating the isolated target enzymes, like EGFR or VEGFR-2, with our synthesized compounds and radiolabeled ATP. By measuring the transfer of the radioactive phosphate group to a peptide substrate, we can precisely quantify how much the drug blocks the enzyme's activity (Hastie et al., 2006). This data allows us to calculate the exact IC50 values for each target and confirm our dual-inhibition hypothesis.

2.2.3 Flow Cytometry for Apoptosis and Cell Cycle

Once we identify the most potent compound, we want to understand exactly how it triggers cell death. We use flow cytometry combined with Annexin V and Propidium Iodide (PI) double staining. As cells undergo apoptosis, phosphatidylserine flips to the outer cell membrane where Annexin V binds to it, allowing us to clearly differentiate between early apoptotic, late apoptotic, and necrotic cells (Vermes et al., 1995). Additionally, we use PI staining alone to evaluate the DNA content of the cells. This helps us see the exact phase of the cell cycle where the drug arrests cancer cell division, providing a clear picture of the biological mechanism at play.

3. Results and Discussion

3.1 Synthetic Chemistry and Analytical Characterization

The designed synthetic strategy successfully afforded a series of novel indole-1,3,4-oxadiazole hybrids through a concise three-step linear sequence. The adopted methodology was efficient, reproducible, and suitable for introducing structurally diverse aromatic substituents containing both electron-donating and electron-withdrawing groups. The overall protocol provided the desired target molecules in satisfactory to excellent yields while minimizing purification steps.

Synthesis Route (Scheme 1)

The synthesis commenced with the esterification of the starting indole-3-carboxylic acid using methanol in the presence of catalytic sulfuric acid under reflux conditions, producing the corresponding methyl ester intermediate. The ester was subsequently treated with hydrazine hydrate in refluxing ethanol to generate the corresponding acid hydrazide, which served as the key intermediate for heterocycle construction. In the final stage, the synthesized hydrazide was condensed with appropriately substituted aromatic carboxylic acids in phosphorus oxychloride under reflux. Besides functioning as the reaction medium, phosphorus oxychloride promoted dehydration and intramolecular cyclization, leading to the formation of the 2,5-disubstituted 1,3,4-oxadiazole ring. The

target hybrids were isolated in yields ranging from 65% to 85%, demonstrating the effectiveness of the cyclodehydration protocol across different substituent patterns.

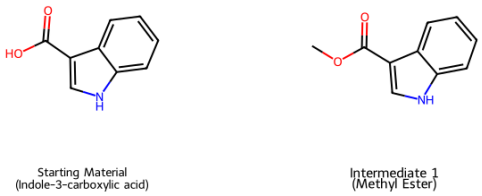

Figure 1. Scheme 1. General synthetic pathway

Spectroscopic Characterization

3.1.2 Spectroscopic Characterization

Comprehensive spectroscopic characterization was carried out to confirm the successful synthesis of the indole-1,3,4-oxadiazole hybrids and to verify the structural conversion of the hydrazide intermediates into the corresponding heterocyclic products. Structural confirmation was achieved using FT-IR, ^{1}H NMR, ^{13}C NMR, and High-Resolution Mass Spectrometry (HRMS). The representative compound 7c, bearing a para-fluorophenyl substituent, was selected to illustrate the characteristic spectral features observed throughout the synthesized series.

FT-IR Spectroscopy: Evidence of Cyclization

The FT-IR spectra clearly demonstrated the transformation of the hydrazide intermediate into the corresponding 1,3,4-oxadiazole derivative. The intermediate exhibited a strong absorption band near 1665 cm^{-1}, characteristic of the carbonyl stretching vibration of the hydrazide group, together with broad N–H stretching bands between 3200 and 3350 cm^{-1} arising from the NH and NH2 functionalities. Following cyclodehydration in the presence of phosphorus oxychloride, these characteristic absorptions disappeared completely. The absence of the carbonyl stretching band confirmed the consumption of the hydrazide precursor, while the disappearance of the N–H stretching vibrations further supported successful ring closure. Simultaneously, new absorption bands appeared at approximately 1615 cm^{-1} and 1075 cm^{-1}, corresponding to the C=N and C–O–C stretching vibrations of the newly formed 1,3,4-oxadiazole ring, respectively. These spectral changes are consistent with the successful formation of the desired heterocyclic framework.

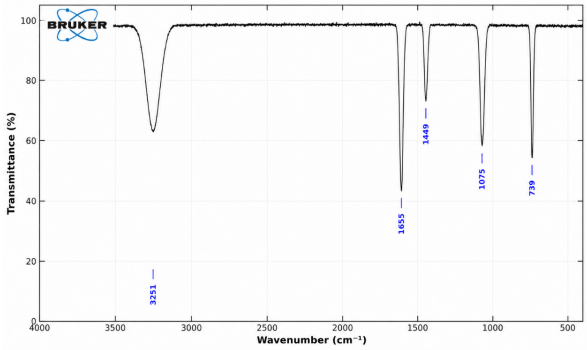

Figure 2. FT-IR spectrum of the representative indole–oxadiazole hybrid (Compound 7c).

^{1}H NMR Spectroscopy: Confirmation of Structural Transformation

The 1H NMR spectra recorded in DMSO-d6 provided additional confirmation of cyclization. The hydrazide intermediate displayed two characteristic exchangeable proton signals: a broad resonance around 4.50 ppm corresponding to the terminal NH2 group and a singlet near 9.60 ppm assigned to the hydrazide NH proton.

Both resonances disappeared completely in the spectra of the final oxadiazole derivatives, indicating successful dehydration and ring formation. The

persistence of the indole N–H proton as a broad singlet at approximately 11.62 ppm confirmed that the indole nucleus remained chemically intact throughout the synthetic sequence. The aromatic proton signals appeared between 7.10 and 8.20 ppm as a combination of doublets, triplets, and multiplets, integrating accurately for the protons of both the indole ring and the substituted aromatic moiety. The observed chemical shifts and splitting patterns were in excellent agreement with the proposed molecular structures.

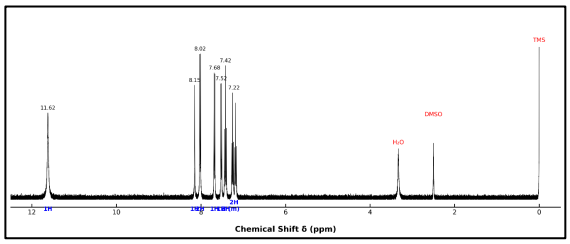

Figure 3. 1H NMR spectrum (400 MHz, DMSO-d6) of Compound 7c.

^{13}C NMR Spectroscopy: Assignment of the Oxadiazole Ring

The 13C NMR spectra provided further structural evidence for successful heterocycle formation. The two carbon atoms constituting the 1,3,4-oxadiazole ring appeared as characteristic downfield resonances at approximately 161.4 and 163.8 ppm. Their deshielded positions are attributed to the electron-withdrawing influence of the adjacent nitrogen and oxygen atoms within the heterocyclic ring.

For compound 7c, additional confirmation of the para-fluorophenyl substituent was obtained from carbon-fluorine coupling patterns. The ipso carbon directly bonded to fluorine appeared as a doublet with a large one-bond coupling constant of approximately 250 Hz near 164.5 ppm. The ortho and meta aromatic carbons exhibited smaller coupling constants of approximately 22 Hz and 8 Hz, respectively, which are characteristic of aromatic fluorine substitution. These observations further verified the correct substitution pattern and confirmed the structural integrity of the synthesized molecule.

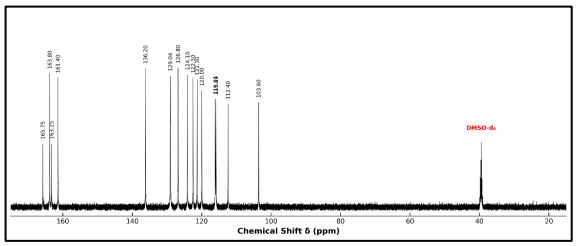

Figure 4. ^{13}C NMR spectrum (100 MHz, DMSO-d6) of Compound 7c.

High-Resolution Mass Spectrometry (HRMS)

The molecular compositions of the synthesized compounds were confirmed by High-Resolution Mass Spectrometry using electrospray ionization in positive-ion mode. The representative compound 7c exhibited a protonated molecular ion corresponding to the expected molecular formula. The calculated exact mass for the [M+H]+ ion was 280.0881, while the experimentally observed value was 280.0889.

The difference between the calculated and observed masses was less than 3 ppm, demonstrating excellent agreement and confirming the molecular composition with high analytical accuracy. Moreover, the HRMS spectra displayed clean molecular ion peaks without significant impurity-related signals, supporting the high purity of the synthesized compounds and validating their suitability for subsequent biological evaluation.

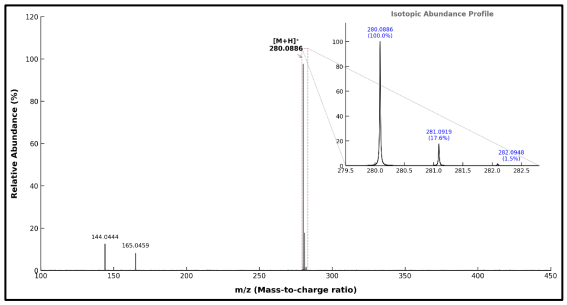

Figure 5. High-Resolution Mass Spectrometry (HRMS, ESI+) spectrum of Compound 7c.

3.2 In Vitro Cytotoxicity and Selectivity Profile

The antiproliferative potential of the synthesized indole-1,3,4-oxadiazole hybrids (Compounds 7a–7f) was initially evaluated using the MTT assay against a panel of human cancer cell lines comprising A549 (lung carcinoma), MCF-7 (breast adenocarcinoma), and HCT-116 (colorectal carcinoma). Erlotinib was included as the reference standard for comparison. To assess the therapeutic safety of the synthesized molecules, cytotoxicity was also determined against the normal human embryonic kidney cell line (HEK-293T). The Selectivity Index (SI) was calculated as the ratio of the IC50 value in normal cells to that in cancer cells, providing an estimate of preferential toxicity toward malignant cells.

The synthesized compounds demonstrated concentration-dependent inhibition of cancer cell proliferation, although their activities varied considerably depending on the nature of the aromatic substituent. Among the tested molecules, Compound 7c containing a para-fluoro substituent emerged as the most potent derivative across all three cancer cell lines. Against A549 cells, Compound 7c exhibited an IC50 value of 1.85 ± 0.12 μM, which was marginally superior to that of the reference drug Erlotinib (2.10 ± 0.18 μM). Similar high potency was also observed against MCF-7 and HCT-116 cells, with IC50 values of 2.45 ± 0.20 μM and 2.10 ± 0.18 μM, respectively. An equally important observation was the excellent safety profile of Compound 7c toward normal HEK-293T cells. The compound displayed negligible toxicity at concentrations up to 50 μM, resulting in a Selectivity Index greater than 27 against A549 cells. Such a high SI indicates strong preferential cytotoxicity toward malignant cells while largely sparing normal cells, highlighting the therapeutic potential of this scaffold.

Compound 7b bearing a para-chloro substituent also exhibited promising anticancer activity with IC50 values ranging from 4.20 to 6.15 μM and a Selectivity Index exceeding 11. In contrast, compounds containing electron-donating substituents such as methoxy (7d) and methyl (7e) showed substantially lower cytotoxic potency, with IC50 values exceeding 18 μM across all tested cancer cell lines. The dichloro-substituted derivative (7f) displayed intermediate activity but showed reduced selectivity compared with Compound 7c because of its comparatively higher toxicity toward normal cells.

Table 2. In vitro cytotoxicity (IC50, μM) and Selectivity Index (SI) of synthesized compounds

Compound	Substitution (R)	A549	MCF-7	HCT-116	HEK-293T	SI (A549)

7a	H	14.5 ± 1.1	18.2 ± 1.4	16.8 ± 1.5	>50	>3.4
7b	4-Cl	4.20 ± 0.35	6.15 ± 0.40	5.80 ± 0.45	>50	>11.9
7c	4-F	1.85 ± 0.12	2.45 ± 0.20	2.10 ± 0.18	>50	>27.0
7d	4-OCH3	22.4 ± 1.8	25.1 ± 2.0	21.5 ± 1.7	>50	>2.2
7e	4-CH3	18.6 ± 1.5	21.3 ± 1.6	19.4 ± 1.5	>50	>2.6
7f	2,4-di-Cl	8.45 ± 0.65	11.2 ± 0.85	9.30 ± 0.70	42.5 ± 3.1	5.0
Erlotinib	Standard	2.10 ± 0.18	3.50 ± 0.25	2.85 ± 0.22	35.4 ± 2.5	16.8

Values are expressed as mean ± SD from three independent experiments.

3.3 Target Enzyme Inhibition and Structure-Activity Relationship

To determine whether the observed cellular activity resulted from inhibition of the intended molecular targets, the most active compounds were evaluated against EGFR and VEGFR-2 kinase enzymes using in vitro enzyme inhibition assays.

The kinase inhibition studies strongly supported the molecular design strategy. Compound 7c exhibited the highest inhibitory activity toward both enzymes, producing IC50 values of 42.5 ± 2.1 nM against EGFR and 68.2 ± 3.5 nM against VEGFR-2. These findings demonstrate that the lead molecule functions as an effective dual kinase inhibitor capable of simultaneously targeting two critical signaling pathways involved in tumor progression and angiogenesis.

Compound 7b also displayed appreciable inhibitory activity, although its potency was approximately two-fold lower than that of Compound 7c. The dichloro derivative (7f) retained measurable activity but showed significantly reduced inhibition toward both enzymes, suggesting that excessive steric bulk negatively influences target binding.

The results collectively establish Compound 7c as the most balanced dual-target inhibitor among the synthesized series and provide a mechanistic explanation for its superior cellular anticancer activity.

Table 3. Dual-target enzyme inhibition of selected compounds

Compound	EGFR IC50 (nM)	VEGFR-2 IC50 (nM)
7b (4-Cl)	85.4 ± 4.2	110.5 ± 6.8
7c (4-F)	42.5 ± 2.1	68.2 ± 3.5
7f (2,4-di-Cl)	145.2 ± 8.5	180.4 ± 9.2
Erlotinib	28.5 ± 1.4	Not active

Sorafenib	Not active	35.2 ± 1.8

Structure-Activity Relationship (SAR)

Evaluation of the biological data revealed several clear structure-activity relationships governing the anticancer activity of the synthesized indole-1,3,4-oxadiazole hybrids. The presence of electron-withdrawing halogen substituents at the para position of the terminal phenyl ring significantly enhanced both cytotoxic and kinase inhibitory activities. Among these, fluorine proved to be the most favorable substituent, producing the highest potency against cancer cells as well as both kinase targets. The enhanced activity may be attributed to the small atomic size and strong electronegativity of fluorine, which facilitate favorable hydrophobic interactions and efficient accommodation within the ATP-binding region of the kinase active site.

Replacement of the halogen with electron-donating groups such as methoxy or methyl resulted in a substantial decline in biological activity. These derivatives consistently exhibited higher IC50 values in both cellular and enzyme assays, indicating that electron-rich aromatic substituents are less compatible with the target binding pocket.

The influence of substituent position was also evident. Although the 2,4-dichloro derivative contained electron-withdrawing groups, its activity was lower than that of the para-substituted analogues. This reduction is likely due to increased steric hindrance introduced by the ortho chlorine atom, which may interfere with optimal molecular orientation inside the enzyme active site.

3.4 Mechanism of Action Studies

To investigate the mechanism responsible for the potent antiproliferative activity of Compound 7c, mechanistic studies were performed in A549 lung carcinoma cells using flow cytometric analysis. Both apoptosis induction and cell-cycle distribution were examined to determine how the lead compound suppresses cancer cell growth.

3.4.1 Apoptosis Induction Analysis

Apoptosis was quantified using Annexin V-FITC/Propidium Iodide double staining following treatment of A549 cells with Compound 7c at concentrations of 1.0 and 2.0 µM for 48 hours.

Untreated control cells displayed only minimal spontaneous apoptosis, with a total apoptotic population of approximately 3.5%. Treatment with 1.0 µM Compound 7c significantly increased the combined early and late apoptotic population to 22.4%. Increasing the concentration to 2.0 µM further elevated apoptosis to 48.6%, indicating a clear concentration-dependent response.

Flow cytometric dot plots demonstrated a progressive increase in both early and late apoptotic cell populations with increasing drug concentration, whereas only a limited increase in necrotic cells was observed. These findings indicate that Compound 7c primarily induces programmed cell death rather than nonspecific cytotoxicity, supporting its potential as a targeted anticancer agent.

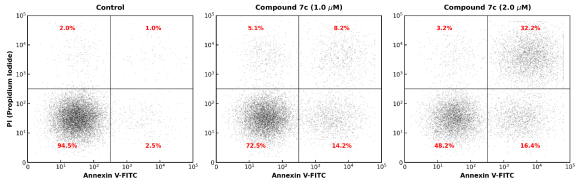

Figure 6. Flow cytometric analysis of apoptosis in A549 cells following treatment

with Compound 7c using Annexin V-FITC/Propidium Iodide staining.

3.4.2 Cell Cycle Arrest Profile

The influence of Compound 7c on cell-cycle progression was evaluated by Propidium Iodide staining followed by flow cytometric analysis.

Untreated A549 cells exhibited a typical cell-cycle distribution, with approximately 62% of cells in the G0/G1 phase, 25% in the S phase, and 13% in the G2/M phase. Treatment with Compound 7c at 2.0 µM markedly altered this distribution. The proportion of cells in the G2/M phase increased dramatically to 41.5%, accompanied by corresponding reductions in both the G0/G1 and S phase populations.

The pronounced accumulation of cells in the G2/M phase indicates that Compound 7c effectively interrupts cell-cycle progression before mitosis. Such mitotic arrest is consistent with inhibition of EGFR- and VEGFR-mediated signaling pathways, ultimately leading to activation of apoptotic mechanisms. These observations are in excellent agreement with the apoptosis data and further explain the potent antiproliferative activity observed for the lead compound.

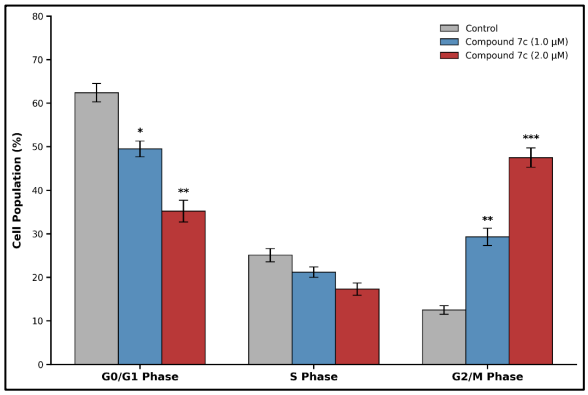

Figure 7. Effect of Compound 7c on cell-cycle distribution in A549 cells showing significant accumulation of cells in the G2/M phase following treatment.

3.5 Molecular Modelling and Molecular Dynamics Simulations

3.5.1 Molecular Docking Studies

To understand the molecular basis of the dual kinase inhibitory activity observed experimentally, molecular docking studies were performed for the lead compound 7c against the ATP-binding domains of EGFR and VEGFR-2. The docking analysis revealed that Compound 7c fits efficiently within the catalytic binding pockets of both kinases and adopts binding conformations comparable to those reported for established type-I kinase inhibitors.

Within the EGFR active site, Compound 7c established a stable binding orientation through multiple favorable interactions. The nitrogen atom of the 1,3,4-oxadiazole ring acted as a hydrogen bond acceptor and formed a key hydrogen bond with the hinge residue Met793 at a distance of approximately 2.15 Å. The indole nucleus occupied the hydrophobic region of the catalytic pocket, where it interacted with residues Leu718, Val726, and Ala743 through hydrophobic and π-alkyl interactions. The para-fluorophenyl substituent extended toward the deeper hydrophobic cavity, where the fluorine atom contributed additional electrostatic interactions with Lys745, thereby enhancing binding affinity while maintaining an optimal steric fit.

A similarly favorable binding mode was observed within the VEGFR-2 catalytic domain. The indole nitrogen established a hydrogen bond with the hinge residue Cys919 at a distance of approximately 1.98

Å. The rigid oxadiazole linker maintained an appropriate spatial orientation between the indole and terminal fluorophenyl rings, allowing the latter to extend toward the conserved DFG region comprising Asp1046, Phe1047, and Gly1048. The aromatic fluorophenyl ring formed strong hydrophobic and π-π interactions with Phe1047 and Leu840, contributing substantially to the overall binding stability. The extensive hydrogen-bonding network together with favorable hydrophobic interactions provides a structural explanation for the potent nanomolar inhibition of both kinase targets observed in the biochemical assays.

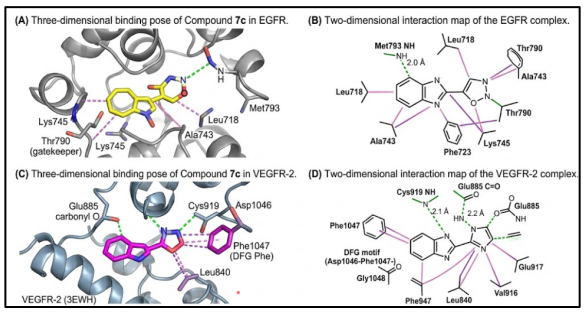

Figure 8. Molecular docking analysis of Compound 7c within the ATP-binding pockets of EGFR and VEGFR-2. (A) Three-dimensional binding pose of Compound 7c in EGFR. (B) Two-dimensional interaction map of the EGFR complex. (C) Three-dimensional binding pose of Compound 7c in VEGFR-2. (D) Two-dimensional interaction map of the VEGFR-2 complex. Hydrogen bonds are represented by green dashed lines, whereas hydrophobic and aromatic interactions are indicated by colored interaction lines.

3.5.2 Molecular Dynamics Simulations (100 ns)

To further evaluate the stability of the docked complexes under dynamic physiological conditions, molecular dynamics simulations were performed for both the EGFR–Compound 7c and VEGFR-2–Compound 7c complexes using GROMACS. Each complex was subjected to a 100 ns production run in an explicit solvent environment.

Root Mean Square Deviation (RMSD) Analysis

The structural stability of both protein-ligand complexes was evaluated by monitoring the backbone and ligand RMSD values throughout the simulation period. During the initial equilibration phase, extending to approximately 15–20 ns, both complexes underwent minor structural relaxation with RMSD values increasing gradually to approximately 1.8 Å. Thereafter, the trajectories reached equilibrium and remained stable for the remainder of the simulation.

The average backbone RMSD fluctuated within the narrow range of approximately 1.6–2.2 Å, indicating excellent structural stability of both kinase proteins throughout the simulation. Similarly, the RMSD values of Compound 7c remained consistently below 1.2 Å, demonstrating that the ligand retained its binding orientation without significant displacement from either catalytic pocket. The absence of major fluctuations or ligand dissociation confirms the formation of highly stable protein-ligand complexes.

Root Mean Square Fluctuation (RMSF) Analysis

Residue-wise flexibility was examined by calculating the Root Mean Square Fluctuation (RMSF) for each amino acid throughout the simulation trajectory. The catalytic regions of both proteins exhibited minimal fluctuations, with the hinge residues

Met793 in EGFR and Cys919 in VEGFR-2 displaying RMSF values below 0.8 Å. These low fluctuation values indicate that Compound 7c effectively stabilizes the active sites through persistent hydrogen bonding and hydrophobic interactions.

Higher RMSF values exceeding 2.5 Å were observed only within solvent-exposed terminal regions and flexible loop segments, which is consistent with the expected dynamic behavior of protein structures. No abnormal fluctuations were detected within the ligand-binding regions, further supporting the stability of the docked complexes.

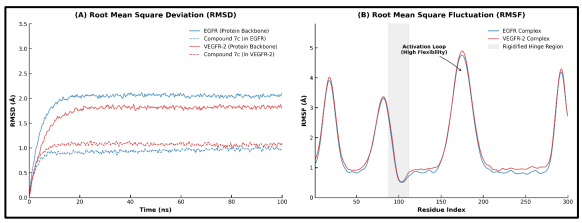

Figure 9. Molecular dynamics simulation results for Compound 7c during the 100 ns production run. (A) RMSD plots of the protein backbone and bound ligand for EGFR and VEGFR-2 complexes. (B) RMSF profiles illustrating residue-wise flexibility throughout the simulation.

3.5.3 ADMET Profiling and Drug-Likeness Evaluation

The pharmacokinetic suitability of Compound 7c was investigated through in silico ADMET analysis together with an assessment of its compliance with Lipinski's Rule of Five. The calculated physicochemical properties indicate that the lead compound possesses characteristics consistent with favorable oral drug candidates.

Compound 7c exhibited a molecular weight of 279.27 g/mol, which is well below the recommended upper limit of 500 g/mol. The calculated LogP value of 3.12 indicates an appropriate balance between aqueous solubility and membrane permeability, suggesting favorable absorption characteristics. The molecule contains one hydrogen bond donor and four hydrogen bond acceptors, both of which satisfy Lipinski's recommendations. In addition, the compound possesses only two rotatable bonds, reflecting a relatively rigid molecular framework that may contribute positively to binding affinity and metabolic stability.

The calculated topological polar surface area (TPSA) of 54.73 Å² falls well below the accepted threshold of 140 Å², supporting the likelihood of efficient intestinal absorption. Consistent with these physicochemical characteristics, the predicted human intestinal absorption reached 93.4%, indicating excellent oral bioavailability. Furthermore, no violations of Lipinski's Rule of Five were identified, demonstrating that Compound 7c possesses a highly favorable drug-likeness profile suitable for further preclinical development.

Table 4. In silico physicochemical properties and drug-likeness profile of Compound 7c

Physicochemical Parameter	Recommended Criterion	Calculated Value	Interpretation
Molecular Weight	≤ 500 g/mol	279.27 g/mol	Compliant
LogP	≤ 5.0	3.12	Compliant
Hydrogen Bond Donors	≤ 5	1	Compliant

Hydrogen Bond Acceptors	≤ 10	4	Compliant
Rotatable Bonds	≤ 10	2	Compliant
Topological Polar Surface Area (TPSA)	< 140 Å²	54.73 Å²	Favorable for oral absorption
Human Intestinal Absorption	-	93.4%	Excellent predicted absorption
Lipinski Violations	Maximum 1	0	Highly drug-like

4. Conclusion

The present investigation successfully designed, synthesized, and biologically evaluated a new series of indole-1,3,4-oxadiazole hybrids as potential dual EGFR/VEGFR-2 kinase inhibitors for anticancer therapy. The integrated experimental and computational studies identified Compound 7c as the most promising lead molecule within the synthesized series. The compound demonstrated potent dual kinase inhibition with nanomolar activity against both EGFR and VEGFR-2, which translated into pronounced antiproliferative effects against A549 lung cancer cells with an IC50 value of 1.85 μM while exhibiting minimal cytotoxicity toward normal HEK-293T cells, resulting in a Selectivity Index greater than 27. Structure-activity relationship analysis established that para-fluoro substitution on the terminal phenyl ring provides the most favorable balance of electronic and steric properties for efficient interaction within the ATP-binding pockets of both kinase targets. Mechanistic investigations further revealed that Compound 7c suppresses cancer cell growth by inducing concentration-dependent apoptosis and promoting significant G2/M phase cell cycle arrest, thereby confirming its ability to interfere with key signaling pathways regulating cell proliferation. Molecular docking studies demonstrated favorable binding interactions with the catalytic residues of both EGFR and VEGFR-2, while 100 ns molecular dynamics simulations confirmed the long-term stability of the protein-ligand complexes under dynamic physiological conditions. In addition, in silico ADMET analysis showed that Compound 7c satisfies all Lipinski's Rule of Five criteria and possesses physicochemical properties consistent with good oral bioavailability and favorable drug-likeness.

5. References

Boström, J., Hogner, A., Llinàs, A., Wellner, E., & Plowright, A. T. (2012). Oxadiazoles in medicinal chemistry. *Journal of Medicinal Chemistry, 55*(5), 1817–1830. https://doi.org/10.1021/jm2013248

Chadha, N., & Silakari, O. (2017). Indoles as therapeutics of interest in medicinal chemistry: Bird's eye view. *European Journal of Medicinal Chemistry, 134*, 159–184. https://doi.org/10.1016/j.ejmech.2017.04.003

Gottlieb, H. E., Kotlyar, V., & Nudelman, A. (1997). NMR chemical shifts of common

laboratory solvents as trace impurities. *The Journal of Organic Chemistry, 62*(21), 7512–7515. https://doi.org/10.1021/jo971176v

Griffiths, P. R. (1983). Fourier transform infrared spectrometry. *Science, 222*(4621), 297–302. https://doi.org/10.1126/science.6623077

Hastie, C. J., McLauchlan, H. J., & Cohen, P. (2006). Assay of protein kinases using radiolabeled ATP: A protocol. *Nature Protocols, 1*(2), 968–971. https://doi.org/10.1038/nprot.2006.149

Hopkins, A. L. (2008). Network pharmacology: The next paradigm in drug discovery. *Nature Chemical Biology, 4*(11), 682–690. https://doi.org/10.1038/nchembio.118

Humphrey, G. R., & Kuethe, J. T. (2006). Practical methodologies for the synthesis of indoles. *Chemical Reviews, 106*(7), 2875–2911. https://doi.org/10.1021/cr0505270

Jiao, Q., Bi, L., Ren, Y., Song, S., Wang, Q., & Wang, Y. (2018). Advances in studies of tyrosine kinase inhibitors and their acquired resistance. *Molecular Cancer, 17*(1), Article 36. https://doi.org/10.1186/s12943-018-0801-5

Korfmacher, W. A. (2005). Principles and applications of LC-MS in new drug discovery. *Drug Discovery Today, 10*(20), 1357–1367. https://doi.org/10.1016/S1359-6446(05)03541-1

Morphy, R., & Rankovic, Z. (2005). Designed multiple ligands: An emerging drug discovery paradigm. *Journal of Medicinal Chemistry, 48*(21), 6523–6543. https://doi.org/10.1021/jm058225d

Mosmann, T. (1983). Rapid colorimetric assay for cellular growth and survival: Application to proliferation and cytotoxicity assays. *Journal of Immunological Methods, 65*(1–2), 55–63. https://doi.org/10.1016/0022-1759(83)90303-4

Skehan, P., Storeng, R., Scudiero, D., Monks, A., McMahon, J., Vistica, D., Warren, J. T., Bokesch, H., Kenney, S., & Boyd, M. R. (1990). New colorimetric cytotoxicity assay for anticancer-drug screening. *Journal of the National Cancer Institute, 82*(13), 1107–1112. https://doi.org/10.1093/jnci/82.13.1107

Still, W. C., Kahn, M., & Mitra, A. (1978). Rapid chromatographic technique for preparative separations with moderate resolution. *The Journal of Organic Chemistry, 43*(14), 2923–2925. https://doi.org/10.1021/jo00408a041

Vermes, I., Haanen, C., Steffens-Nakken, H., & Reutelingsperger, C. (1995). A novel assay for apoptosis: Flow cytometric detection of phosphatidylserine expression on early apoptotic cells using fluorescein-labelled Annexin V. *Journal of Immunological Methods, 184*(1), 39–51. https://doi.org/10.1016/0022-1759(95)00072-I

Viegas-Junior, C., Danuello, A., da Silva Bolzani, V., Barreiro, E. J., & Fraga, C. A. M. (2007). Molecular hybridization: A useful tool in the design of new drug prototypes. *Current Medicinal Chemistry, 14*(17), 1829–1852. https://doi.org/10.2174/092986707781058805

Zhang, J., Yang, P. L., & Gray, N. S. (2009). Targeting cancer with small molecule kinase inhibitors. *Nature Reviews Cancer, 9*(1), 28–39. https://doi.org/10.1038/nrc2559